Mechanical Systems and Signal Processing 130 (2019) 41–55

Contents lists available at ScienceDirect

Mechanical Systems and Signal Processing

journal homepage: www.elsevier.com/locate/ymssp

Path-tracking of autonomous vehicles using a novel adaptive robust exponential-like-sliding-mode fuzzy type-2 neural network controller

Hamid Taghavifar *, Subhash Rakheja

CONCAVE Research Center, Department of Mechanical, Industrial and Aerospace Engineering, Concordia University, Montreal, QC H3G 1M8, Canada

ARTICLE INFO

Article history:
Received 21 January 2019
Received in revised form 30 March 2019
Accepted 28 April 2019
Available online 8 May 2019

Keywords:
Fuzzy system
Lane keeping control
Robustness
Autonomous vehicles

ABSTRACT

Structured and unstructured uncertainties together with external disturbances may pose considerable challenges in realizing desired path-tacking and lane keeping of autonomous vehicles. This paper presents a novel robust adaptive indirect control method based on an exponential-like-sliding-mode fuzzy type-2 neural network approach for enhanced path-tracking performance of road autonomous vehicles subject to parametric uncertainties related to vehicle nominal cornering stiffness, road-tire adhesion coefficient, inertial parameters, and forward speed. A hierarchical controller is designed and the stability of the closed-loop system is ensured along with deriving the adaptation laws by employing the Lyapunov stability theorem. The conventional reaching law related to the sliding mode degrades from the system stability and introduces an inherent chattering of the controller input. The convergence law for the sliding surface is adjusted based on a variable exponential sliding manifold to eliminate possible chattering in the buffeting switch zone near the origin. The proposed exponential-like sliding surface guarantees the swift and smooth global asymptotic convergence of the tracking error toward zero. Furthermore, an adaptive look-ahead path-tracking error term is introduced as an auxiliary error criterion to improve the vehicle path-tracking performance. The effectiveness of the proposed controller is verified through Matlab/Simulink–CarSim co-simulations and comparisons with selected reported control methods for two different road maneuvers. The results suggested substantially improved tracking performance by the proposed controller with robustness to withstand against the perturbed parameters and external disturbances.

1. Introduction

Past few decades have witnessed substantial progress in the field of autonomous vehicles due to the technological growth in cyber-physical systems, advanced control paradigms, and artificial intelligence techniques [1–3]. Human safety, ease of ride, security, and driving accuracy in conjunction with energy and time efficiency in transportation systems have served as primary incentives for additional research efforts leading to design and commercialization of fully automated and connected vehicles, advanced driving-assist systems (ADAS) and parallel steering control [4,5]. However, the complexities related to the road condition and modern urban infrastructure components in addition to the exacerbated trafficking status,

* Corresponding author.
E-mail address: h_taghav@encs.concordia.ca (H. Taghavifar).

https://doi.org/10.1016/j.ymssp.2019.04.060
0888-3270/

have imposed the practice of the state-of-the-art frameworks for autonomous road vehicles [6,7]. Autonomous vehicles are expected to effectively uphold the principal functionalities such as obstacle avoidance, decision making, lane keeping, and motion planning, etc., among which, lateral path-following is the most essential performance measure of autonomous vehicles to ensure vehicle and passenger safety, and lateral motion stability [8–10].

The constraints on the vehicle states and the geometrical/dynamic status of the adjacent vehicles, pedestrians and their unpredictable responses together with the structured or unmodeled uncertainties and external disturbances contribute to extreme complexities for the controller design. A desired lane-keeping performance is achieved by minimizing the errors in terms of the lateral offset and the heading error of the vehicle under varying driving conditions [11–13]. Hence, the principal purpose in the design of control laws is to ensure the lateral offset and the heading error toward zero, while preserving vehicle stability under different maneuver and road conditions. For relatively smooth paths and the explicit system dynamics, the class of classical feedback control laws can typically deliver desirable responses reasonably well [14]. However, an incorrect feedback law can be generated leading to a critical instability when the system dynamics is not fully known, the road path is highly curved or there are maneuvers demanding swift yaw stabilization the road [14]. Robust control methods considering the unknown dynamics of the system are thus vital for ensuring lane-keeping of the autonomous vehicles.

Reported studies have employed wide ranges of control schemes for enhancement of lateral path-tracking or lane-keeping performance of autonomous vehicles such as composite nonlinear feedback [15], adaptive neural network [16], robust H_∞ output-feedback control [17], terminal sliding mode [18], and model predictive control (MPC/NMPC) [19,20], as well as robust controllers for fault detection [21] and nonlinear controls for trajectory-following of electric ground vehicles [21,22]. The effectiveness of a class of controllers such as optimal control and invariants of predictive control strongly relies on the availability of an accurate explicit model describing the system. The models of the autonomous vehicle, however, are generally subject to parametric uncertainties and unmodeled disturbances, which may adversely influence the effectiveness of the optimal and model predictive controllers. A number of studies have thus proposed robust controller designs for the path-tracking of autonomous vehicles. Du and Tan [23] developed a vision-based path-planning module for the autonomous vehicle using a sliding mode controller coupled with the Kalman Filter for state estimation. The steering wheel angle was considered as the controller input for the sliding mode controller and the vehicle position was predicted in real-time using the Kalman filter and image processing techniques. The stability and robustness of the proposed controller was verified for the sliding mode controller. Similarly, an integral sliding mode controller was proposed for the parking task of an autonomous four-wheel drive vehicle via real-time model identification considering the input constraints [24]. A compact-form dynamic linearization observer was considered in the model identification stage and for the integral sliding-mode controller purpose a dynamic integration wind-up resistive compensator was introduced to tackle the integral saturation drawback for the parking system of the autonomous vehicle. Hu et al. [25] developed a robust composite nonlinear feedback control to enhance the system transient response and also to minimize the steady-state errors related to the path-following performance of the autonomous vehicle due to the controller input saturation. The reported robust sliding mode control methods, however, may exhibit limited effectiveness due to the chattering-like control inputs and strong dependence on the explicit model of the system. Adaptive controllers are typically employed in studies where higher robustness is required to withstand the effects of disturbance and uncertainty [26]. Adaptive intelligent control methods can potentially address the challenge of desired control performance against the system uncertainty by learning to approximate any arbitrary nonlinear and uncertain but bounded model dynamics [27–29].

Fuzzy systems, as a principal class of intelligent controllers, have also been employed in path-following of autonomous road vehicles [30–33]. A T-S fuzzy model with the additional norm-bounded uncertainties based controller was developed for following a relatively smooth path- in the presence of system nonlinearities and parametric uncertainties related to variations in vehicle mass and vehicle speed [31]. An adaptive fuzzy observer-based output feedback (AFS) control was designed using the Lyapunov stability theorem for the path-following of autonomous vehicle. Another study employed a similar control strategy using AFS as the control input together with a cascade structure for lateral path-following control and parametric trajectory along a roundabout. Hwang et al. [33] employed a two-stage fuzzy dynamic sliding-mode path-following control comprising a virtual desired input stage and the path tracking control stage. The proposed dynamic fuzzy sliding mode controller employed a tuning mechanism to address system uncertainties, particularly the varying payloads, using the Lyapunov theory. Adaptive fuzzy type-1 controllers have been typically employed in these studies, whereas fuzzy type-2 systems exhibit an enhanced level of efficiency for systems subject to parametric uncertainties or external disturbances since the membership functions are also described in a fuzzy manner [34,35].

This study presents a novel robust adaptive indirect control method based on an exponential-like-sliding-mode fuzzy type-2 neural network approach for enhanced path-tracking of autonomous vehicles subjected in the presence of various parametric uncertainties associated with tire cornering stiffness, road-tire adhesion coefficient, and inertial parameters and forward speed of the vehicle. The controller synthesis is realized considering three specific goals: (i) adaptive control of look-ahead lateral offset errors; (ii) smooth global asymptotic convergence of system dynamics to the desired trajectories via a novel switching exponential-like sliding mode surface together with the fuzzy type-2 neural network controller; and (iii) robustness of the controller in view of structured uncertainty and unmodeled disturbances. The globally uniform stability of the autonomous vehicle under elective but bounded neighborhoods of the origin is verified by employing the Lyapunov stability theorem. The effects of variations in the forward speed on the tracking performance are included in the developed framework considering that an adaptive look-ahead error term can minimize the error at various speeds. The remainder of the paper is structured as follows. In Section 2, the formulations describing the kinematics and dynamics of the autonomous

vehicle and the adaptive look-ahead offset error are presented. In Section 3, fuzzy type-2 neural network structure is briefly presented. Section 4 is dedicated to the structure of the proposed adaptive robust exponential-sliding-mode fuzzy-type-2 controller and stability analysis. The simulation results for the proposed controller using the Matlab/Simulink–CarSim co-simulation are presented and discussed in Section 5. The conclusions of the study are briefly summarized in Section 6.

2. Problem formulation and controller design

The path tracking task of autonomous vehicles generally concerns with minimization of the lateral offset error at vehicle center of gravity (*CG*), while preserving the yaw mode stability. For this purpose, it is important to maintain the yaw velocity as close as possible to a value perceived adequate by a skilled driver or desired to closely follow a given trajectory in a stable manner. In this study, an auxiliary term called adaptive look-ahead error ε_F is defined to describe expected lateral offset of the vehicle at a future target point as a function of its forward velocity with respect to a desired trajectory in the shape of an orthogonal projection (Fig. 1). A novel hierarchical control algorithm is designed to minimize the look-ahead offset error by employing the robustness feature of fuzzy type-2 sets considering the effects of the matched and mismatched uncertainties of the autonomous vehicle system.

2.1. Vehicle model

A vehicle model with active front steering (AFS) is considered for formulating the proposed path following control laws. The vehicle model is formulated assuming negligible contribution of the longitudinal traction/braking forces to the vehicle's lateral dynamics at a constant forward speed, where the traction force is balanced by the motion resistances. Furthermore, the model is limited only to lateral and yaw dynamics of the vehicle assuming negligible roll, pitch and vertical motions. Owing to symmetric dynamics of the right- and left-tracks of the vehicle under nearly parallel steering of the front wheels, the widely reported two degrees-of-freedom (DOF) bicycle model is considered (Fig. 1):

$$\begin{aligned} m(\dot{v}_y + \gamma v_x) &= F_{TF} + F_{TR} \\ I_z\dot{\gamma} &= l_1 F_{TF} - l_2 F_{TR} \end{aligned} \tag{1}$$

where m is the vehicle total mass, v_x is the vehicle forward speed, γ is yaw-rate of the vehicle body, v_y is the vehicle lateral speed, I_z is yaw moment of inertia, l_1 and l_2 are distances from (*CG*) to front- and rear-axle, respectively, and F_{TF} and F_{TR} are the lateral forces developed at the front- and rear-axle tires, respectively, given by [36]:

$$\begin{aligned} F_{TF} &= \mu_t C_F \alpha_F \\ F_{TR} &= \mu_t C_R \alpha_R \end{aligned} \tag{2}$$

where μ_t is tire–road adhesion coefficient, $C_F$and C_R are cornering stiffness of front-and rear axle tires, and α_F and α_R are side-slip angles of the front-axle and rear-axle tires, respectively, obtained from:

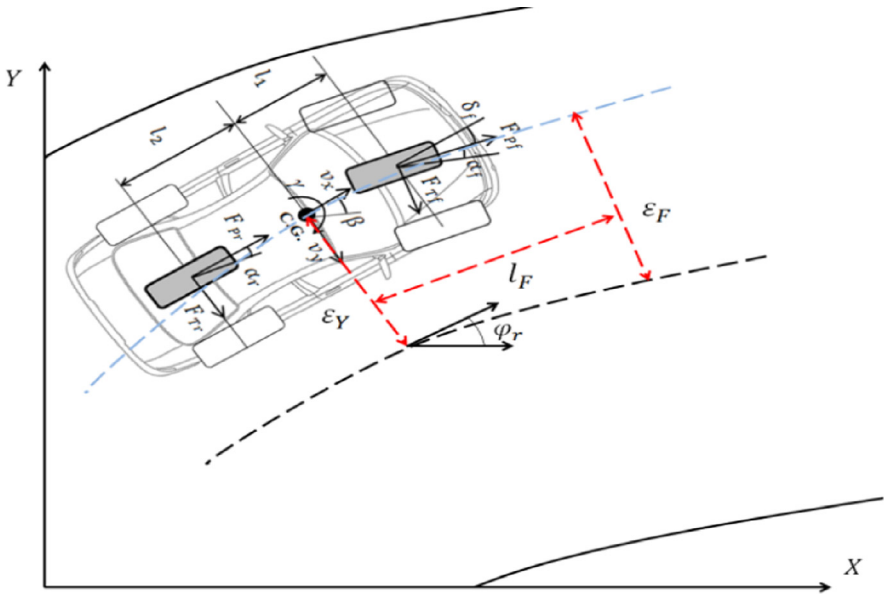

Fig. 1. Yaw-plane vehicle model.

$$\begin{aligned}\alpha_F &= \arctan\left[\frac{v_y+l_1\gamma}{v_x}-\delta_f\right] \cong \beta+\frac{l_1\gamma}{v_x}-\delta_f\\ \alpha_F &= arctan\left[\frac{v_y-l_2\gamma}{v_x}\right] \cong \beta-\frac{l_2\gamma}{v_x}\end{aligned} \tag{3}$$

where δ_f is front wheel steer angle and $\beta = v_y/v_x$ is the vehicle side-slip angle. The cornering stiffness of a tire is known to vary with many operating factors in a highly nonlinear manner such as tire load, road surface adhesion, slip angle, speed and state of tire [13]. The cornering stiffness of the tire is thus defined considering the uncertainties $(\Delta C_F, \Delta C_R)$ due to operating conditions and tire nonlinearity, as:

$$\begin{aligned}C_F &= \widehat{C}_F + \Delta C_F\\ C_R &= \widehat{C}_R + \Delta C_R\end{aligned} \tag{4}$$

where $\widehat{C}_F$ and $\widehat{C}_R$ are nominal cornering stiffness of the front and rear axle tires, respectively. Eqs. (1)–(3) yield the governing relations for lateral speed and yaw-rate in the state-space form, as:

$$\begin{aligned}\dot{v}_y &= \frac{1}{m}\left[\mu_t C_F\left(\beta+\frac{l_1\gamma}{v_x}-\delta_f\right)+\mu_t C_R\left(\beta-\frac{l_2\gamma}{v_x}\right)\right]-\gamma v_x\\ \dot{\gamma} &= \frac{1}{I_z}\left[l_1\mu_t C_F\left(\beta+\frac{l_1\gamma}{v_x}-\delta_f\right)-l_2\mu_t C_R\left(\beta-\frac{l_2\gamma}{v_x}\right)\right]\end{aligned} \tag{5}$$

The time derivatives of lateral and longitudinal offsets in the global (*X*-*Y*) coordinate system, $\dot{\varepsilon}_Y$ and$\dot{\varepsilon}_X$, are obtained as:

$$\begin{aligned}\dot{\varepsilon}_Y &= v_x\sin\Delta\varphi - v_y\cos\Delta\varphi + d_3 \cong v_x\Delta\varphi - v_y\\ \dot{\varepsilon}_X &= v_x\cos\Delta\varphi + v_y\sin\Delta\varphi \cong v_x + v_y\Delta\varphi\end{aligned} \tag{6}$$

Similarly the time derivative of the heading error $\Delta\varphi$, defined as difference between the vehicle heading angle φ and that of the target trajectory φ_r $(\Delta\varphi = \varphi - \varphi_r)$, can be expressed as a function of the vehicle yaw-rate γ:

$$\Delta\dot{\varphi} = \dot{\varphi} - \dot{\varphi}_r = \gamma - \rho(\kappa)\dot{\varepsilon}_X \tag{7}$$

where κ stands for the curvilinear coordinate or arc length of the desired path from an initial predetermined position such that $\kappa \geq 0$, and $\dot{\kappa} = \frac{d\kappa}{dt} \neq 0$. Furthermore, $\rho(\kappa)$ indicates the curvature of the desired trajectory for $t \epsilon R^+$, which varies with the change in distance κ. According to Fig. 1, a lateral offset error term is introduced as a function of vehicle CG lateral offset and the adaptive look-ahead offset error $l_F\sin\Delta\varphi$, as:

$$\varepsilon_F = \frac{1}{2}\left[(\varepsilon_Y)^2 + (l_F\sin\Delta\varphi)^2\right] \cong \frac{1}{2}\left[(\varepsilon_Y)^2 + (\Xi v_x\Delta\varphi)^2\right] \tag{8}$$

where $l_F = \Xi v_x$ and Ξ is the look-ahead time to reach the desired target point l_F in an adaptive manner. By adjusting the vehicle speed, the look-ahead distance can be updated accordingly. The time derivative of (8) can be expressed as:

$$\dot{\varepsilon}_F = (\varepsilon_Y\dot{\varepsilon}_Y + \Xi v_x\Delta\dot{\varphi}) = \left(\varepsilon_Y v_x\Delta\varphi - \varepsilon_Y v_y + \Xi v_x\rho(\kappa)\left[v_x + v_y\Delta\varphi\right]\right) \tag{9}$$

Furthermore, the second time derivative of ε_F can be described as follows.

$$\ddot{\varepsilon}_F = \left(\varepsilon_Y\ddot{\varepsilon}_Y + \Xi v_x\Delta\ddot{\varphi} + {\dot{\varepsilon}_Y}^2\right) \tag{10}$$

Using (6) and (7), the above can be re-written, as:

$$\ddot{\varepsilon}_F = \left(\varepsilon_Y v_x\Delta\dot{\varphi} - \varepsilon_Y\dot{v}_y + \Xi v_x\rho(\kappa)\left[\frac{\dot{\gamma}}{\rho(\kappa)} - \dot{v}_y\Delta\varphi - v_y\Delta\dot{\varphi}\right]\right) + {\dot{\varepsilon}_Y}^2 \tag{11}$$

2.2. Controller design

In this section, a controller is designed for the smooth and global asymptotic convergence of the tracking error related to the autonomous vehicle toward zero by considering the vehicle adaptive look-ahead tracking error. For the robustness analysis of the system, the vehicle model is subjected to parametric uncertainty in addition to unknown but bounded external disturbances. The governing equations for lateral dynamics of the vehicle (5) can be expressed in the generalized form, as:

$$\begin{aligned}\dot{\underline{x}} &= \underline{f}(\underline{x}) + \underline{g}(u) + \boldsymbol{D}\\ \underline{y} &= \boldsymbol{C}\underline{x}\end{aligned} \tag{12}$$

where $\underline{f} = [f_1, f_2]^T$, $\underline{g} = [g_1, g_2]^T$, $f_1 = \frac{1}{m}\left[\mu_t C_F\left(\beta+\frac{l_1\gamma}{v_x}\right)+\mu_t C_R\left(\beta-\frac{l_2\gamma}{v_x}\right)\right]-\gamma v_x$, $g_1 = \frac{-1}{m}\left[\mu_t C_F(\delta_f)\right]$, $f_2 = \frac{1}{I_z}\left[l_1\mu_t C_F\left(\beta+\frac{l_1\gamma}{v_x}\right) - l_2\mu_t C_R\left(\beta-\frac{l_2\gamma}{v_x}\right)\right]$ and, $g_2 = \frac{-1}{I_z}\left[l_1\mu_t C_F(\delta_f)\right]$. Furthermore, $\underline{x} = \left[v_y, \gamma\right]^T$ and $u = \delta_f$ is the control input, $\boldsymbol{C}$ is an identity matrix

and $\boldsymbol{D}$ represents the vector of disturbances incurred by the system. A two-step process for stabilization of the servo controller is formulated.

Step 1. Considering Eq. (8), the tracking error ε_F converging to zero indicates that the vehicle lateral offsets at *CG* and vehicle head point are zero. For this purpose, the design Lyapunov function candidate is selected as:

$$V_1 = \frac{1}{2}{\varepsilon_F}^2 \tag{13}$$

The differentiation of Eq. (13) yields:

$$\dot{V}_1 = \varepsilon_F \dot{\varepsilon}_F \tag{14}$$

Step 2. Let us introduce a switching Lyapunov candidate function V_3, which includes the heading angle error and (14) such that the control law for the stability in the sense of Lyapunov is derived, as:

$$\begin{aligned} V_2 &= \dot{V}_1 \\ V_3 &= \tfrac{1}{2}{V_2}^2 + \tfrac{1}{2}\Delta\varphi^2 \end{aligned} \tag{15}$$

Differentiation of Eq. (15) yields:

$$\dot{V}_3 = V_2\dot{V}_2 + \Delta\varphi\Delta\dot{\varphi} = {\varepsilon_F}^2\dot{\varepsilon}_F\ddot{\varepsilon}_F + \varepsilon_F{\dot{\varepsilon}_F}^3 + \Delta\varphi\Delta\dot{\varphi} \tag{16}$$

By imposing $\dot{V}_3 \leq 0$ for the stability of the system, the above leads to:

$$\dot{V}_3 \leq 0 \rightarrow \ddot{\varepsilon}_F \leq -\left(\frac{\Delta\varphi\Delta\dot{\varphi}}{\varepsilon_F\dot{\varepsilon}_F} + {\dot{\varepsilon}_F}^2\right){\varepsilon_F}^{-1} \tag{17}$$

By combining (11) and (17), the following negative semi-definite control function is derived.

$$(\varepsilon_Y - \Delta\varphi/\rho(\kappa))\dot{v}_y + \Xi v_x\rho(\kappa)\dot{\gamma} \leq -\left(\frac{\Delta\varphi\Delta\dot{\varphi}}{\varepsilon_F\dot{\varepsilon}_F} + {\dot{\varepsilon}_F}^2\right){\varepsilon_F}^{-1} - h_1 \tag{18}$$

where

$$h_1 = \left\{\frac{\varepsilon_Y}{m}\left[\mu_t C_F\left(\beta + \frac{l_1\gamma}{v_x} - \delta_f\right) + \mu_t C_R\left(\beta - \frac{l_2\gamma}{v_x}\right)\right] - \varepsilon_Y v_x(\gamma - \dot{\varepsilon}_X) - {\dot{\varepsilon}_Y}^2 + v_y/\rho(\kappa)(\gamma - \dot{\varepsilon}_X/\rho(\kappa))\right\}$$

Upon substituting for $\dot{v}_y$ and $\dot{\gamma}$ from (5) into (18), the active steering control law is derived as:

$$\delta_f = \left[-\left(\frac{\Delta\varphi\Delta\dot{\varphi}}{\varepsilon_F\dot{\varepsilon}_F} + {\dot{\varepsilon}_F}^2\right){\varepsilon_F}^{-1} - h_1 - h_2\right]{h_3}^{-1} \tag{19}$$

where

$$\begin{aligned} h_2 &= \tfrac{\Delta\varphi - \varepsilon_Y}{m}\left[\mu_t C_F\left(\beta + \tfrac{l_1\gamma}{v_x}\right) + \mu_t C_R\left(\beta - \tfrac{l_2\gamma}{v_x}\right)\right] - (\Delta\varphi - \varepsilon_Y)\gamma v_x + \tfrac{\Xi v_x}{I_z}\left[l_1\mu_t C_F\left(\beta + \tfrac{l_1\gamma}{v_x}\right) + l_2\mu_t C_R\left(\beta - \tfrac{l_2\gamma}{v_x}\right)\right] \\ h_3 &= \left(\tfrac{\Delta\varphi - \varepsilon_Y}{m} - \tfrac{\Xi v_x}{I_z}\right)\mu_t C_F \end{aligned}$$

Choosing the control law in (19) will thus ensure the stability of the function V_3 in (15), implying that:

$$V_2 \wedge \Delta\varphi \triangleq 0;\ \varphi = \varphi_r \wedge \varepsilon_F\dot{\varepsilon}_F = 0 \tag{20}$$

Consequently, the convergence of the heading angle toward the desired trajectory is ensured, while the subsequent term in (20) implies:

$$\varepsilon_F\dot{\varepsilon}_F \triangleq 0;\ \varepsilon_F = 0 \vee \dot{\varepsilon}_F = 0 \tag{21}$$

Above equation can lead to two possible scenarios: i) $\lim_{t\to\infty}\varepsilon_F = 0$ or ii) $\lim_{t\to\infty}\dot{\varepsilon}_F = 0$. The second scenario does not ensure convergence to a zero tracking-error performance of the autonomous vehicle. A switched multi sliding manifold is thus proposed to achieve global asymptotic convergence of the tracking error toward zero. Furthermore, the unknown dynamics of the vehicle are estimated employing the adaptive type-2 fuzzy neural network (T2FNN) controller design, as described below.

3. Description of proposed Type-2 fuzzy neural network (T2FNN)

In this section, a brief description of fuzzy type-2 sets is presented. Fuzzy type-2 systems are more generic invariants of their fuzzy type-1 counterparts, which have been proposed to withstand against strong fuzziness in the determination of the fuzzy membership functions themselves [37]. Fuzzy type-2 systems can be employed in scenarios where it is arduous to determine an exact membership function such as when the training data are corrupted by noise or in the presence of parametric uncertainties in the model. Fig. 2 illustrates the typical Takagi-Sugeno interval type-2 fuzzy Gaussian membership

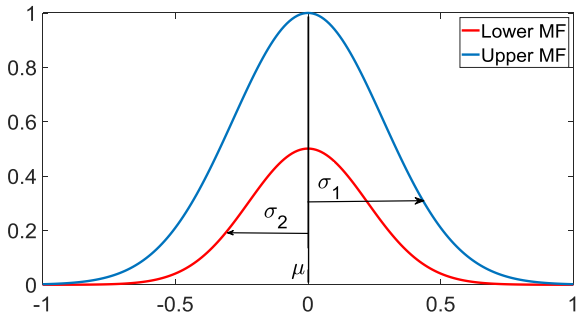

Fig. 2. A typical interval type-2 fuzzy Gaussian membership function with uncertain standard deviations.

functions, where mean is represented by μ and the standard deviations for the upper and lower MFs are denoted by σ_1 and σ_2, respectively. Considering the normal distribution of the state variables about the mean value μ, the Gaussian membership function is employed, while the parameters μ, σ_1 and σ_2 are updated during the adaptation law procedure.

Hereafter, the interval type-2 fuzzy set is presented together with the inference logic system associated with the type-2 fuzzy set. Typically, a fuzzy logic system comprising a minimum of one type-2 fuzzy set is considered as a type-2 fuzzy logic system. The interval type-2 fuzzy set A in domain X can be described as follows [37]:

$$\widetilde{A} = \int_{x\in X} \frac{\left[\int_{u\in J_x} \widetilde{u}^{-1}\right]}{x} \qquad J_x \subseteq [0\ 1] \tag{22}$$

where J_x is the footprint of uncertainty of the fuzzy set A, and x and u are the primary and secondary variables defined in the domain X. The framework of a typical fuzzy type-2 system for given M rules and q inputs can be presented as:

$$\text{Rule}i:\ \text{IF } x_1 \text{ is } \widetilde{A}_1^i \text{ and } x_2 \text{ is } \widetilde{A}_2^i\ \ldots\ x_q \text{ is } \widetilde{A}_q^i \text{ THEN } y \text{ is } \underline{y}^i i = 1, 2,\ \ldots\ , M \tag{23}$$

where $x = (x_1, x_2, \ldots, x_q)$ denotes the input vector to the type-2 fuzzy system, $\left\{\widetilde{A}_1^i, \widetilde{A}_2^i, \ldots, \widetilde{A}_q^i\right\}$ is an interval type-2 fuzzy set, y represents the descendant linguistic variables, and $\underline{y}^i = \left[y_v^i, y_s^i\right]$ is regarded as model output comprising the upper and lower membership functions y_v^i and y_s^i, respectively. The multilayered output of the employed T2FNN system can be expressed as follows:

Layer 1: In this layer, the crisp values are imported to the network as the inputs.

Layer 2: In the second layer, the upper and lower MFs are defined and the outputs of type-2 membership functions are derived. Each of the upper and lower MFs are assigned a degree of membership using the nodes, which carry a certain mean value μ but uncertain standard deviations σ_1 and σ_2 for the upper and lower MFs, respectively, defined as:

$$\overline{\mu}_i^q(x_q) = exp\left(-\frac{1}{2}\left(\frac{x_q - \mu_i^q}{\overline{\sigma}_i^q}\right)^2\right) \tag{24}$$

$$\underline{\mu}_i^q(x_q) = exp\left(-\frac{1}{2}\left(\frac{x_q - \mu_i^q}{\underline{\sigma}_i^q}\right)^2\right)$$

where $\overline{\mu}_i^q(x_q)$ and $\underline{\mu}_i^q(x_q)$ are the upper and lower types of the firing degrees associated with the outputs of *ith* upper and lower membership functions, respectively and the qth input. Additionally, μ_i^q is the mean and $\sigma = \left[\overline{\sigma}_i^q . \underline{\sigma}_i^q\right]$ are of the uncertain widths of the ith upper and lower membership functions for the *qth* input, respectively.

Layer 3: In this layer, where each node is so-called rule node, the product operation is implemented on the inputs from the output of Layer 2 in order to derive the upper and lower firing strengths. The nodes are associated with the rules, where a total of M rules are available for each of the upper and lower functions that define the firing degrees, such that:

$$\bar{\chi}^i(x) = \overline{\mu}_{\widetilde{A}_1^i}(x_1) \times \overline{\mu}_{\widetilde{A}_2^i}(x_2) \times \cdots \overline{\mu}_{\widetilde{A}_q^i}(x_q)$$

$$\underline{\chi}^i(x) = \underline{\mu}_{\widetilde{A}_1^i}(x_1) \times \underline{\mu}_{\widetilde{A}_2^i}(x_2) \times \cdots \underline{\mu}_{\widetilde{A}_q^i}(x_q) \tag{25}$$

where $\overline{\mu}_{\widetilde{A}_1^i}$ and $\underline{\mu}_{\widetilde{A}_1^i}$ are the *ith* upper and lower degrees of membership, respectively.

Layer 4: In this layer, the type-reduction procedure is performed and the outputs y_s and y_v are described according to [38,39]. For the center-of-sets defuzzification method, each rule consequent is determined by a singleton position at its center and the output expression is defined by the Karnek-Mendel-Liang iterative method [39], expressed as:

$$y_s = \frac{\sum_{i=1}^{L} \underline{\chi}^i w_s^i + \sum_{i=L+1}^{M} \bar{\chi}^i w_s^i}{\sum_{i=1}^{L} \underline{\chi}^i + \sum_{i=1}^{M} \bar{\chi}^i}$$

$$y_v = \frac{\sum_{i=1}^{R} \underline{\chi}^i w_v^i + \sum_{i=R+1}^{M} \bar{\chi}^i w_v^i}{\sum_{i=1}^{R} \underline{\chi}^i + \sum_{i=1}^{M} \bar{\chi}^i} \tag{26}$$

where w_v^i and w_s^i are the consequent parameters in the ith rule for the upper and lower firing rules. The parameters R and L are used in the type reduction procedure based on Karnik–Mendel (KM) [39]. As mentioned in the third layer, there are a total of M rules for the upper and lower MFs. Therefore, w_v^i and w_s^i are the weighting factors related to the outputs y_s and y_v, which can be expressed as:

$$w_v^i = \alpha_{q-1}^i + \alpha_q^i x_j + \alpha_{q+1}^i x_{q+1} \cdots$$

$$w_s^i = \underset{\sim}{\beta}_{j-1}^i + \underset{\sim}{\beta}_j^i x_j + \underset{\sim}{\beta}_{j+1}^i \underset{\sim}{x}_{j+1} + \cdots i = 1, 2, \cdots, M;\ q = 1, 2, \cdots, 12 \tag{27}$$

where x_q denotes the inputs to the T2FNN, q is the number of inputs and $\underset{\sim}{\alpha}_j^i$ and $\underset{\sim}{\beta}_j^i$ represent the adaptive parameters corresponding to the *ith* MF and *qth* input that are updated. By assuming $\delta_s = \sum_{i=1}^{L} \underline{\chi}^i + \sum_{i=1}^{M} \bar{\chi}^i$, $\delta_v = \sum_{i=1}^{R} \underline{\chi}^i + \sum_{i=1}^{M} \bar{\chi}^i$, $\underline{Q}_s^i = \underline{\chi}^i / \delta_s$, $\overline{Q}_s^i = \bar{\chi}^i / \delta_s$, $\underline{Q}_v^i = \underline{\chi}^i / \delta_v$, and $\overline{Q}_v^i = \bar{\chi}^i / \delta_v$, (26) can be expressed as:

$$y_s = \sum_{i=1}^{L} \underline{Q}_s^i w_s^i + \sum_{i=L+1}^{M} \overline{Q}_s^i w_s^i = \Theta_s^T \xi_s$$

$$y_v = \sum_{i=1}^{L} \underline{Q}_v^i w_v^i + \sum_{i=L+1}^{M} \overline{Q}_v^i w_v^i = \Theta_v^T \xi_v \tag{28}$$

where $\xi_s^T = \left[\underline{Q}_s^i, \overline{Q}_s^i\right]$, $\Theta_s^T = \left[\underline{w}_s^i, \overline{w}_s^i\right]$, $\xi_v^T = \left[\underline{Q}_v^i, \overline{Q}_v^i\right]$, and $\Theta_v^T = \left[\underline{w}_v^i, \overline{w}_v^i\right]$.

Layer 5: Finally, the outputs are obtained by averaging of the two terms in (28).

$$y = \frac{(y_s + y_v)}{2} = \Theta^T \xi \tag{29}$$

where Θ^T represents a general weight vector and ξ denotes multilayer perceptron vector for estimation of output y according to the upper and lower outputs of T2FNN in (28).

4. Switched multi-sliding manifold T2FNN controller

The unknown and bound-limited functions $\boldsymbol{f}(.)$ and $\boldsymbol{g}(.)$ in (12) together with the control effort, $u(t) \in R$ describe lateral dynamics of the vehicle, while ensuring minimal lateral offset and stability of the closed-loop system. The aforementioned unknown functions can be estimated from a T2FNN system through the respective terms $\widehat{\boldsymbol{f}}\left(\widehat{\boldsymbol{x}}|\boldsymbol{\Theta}_{\boldsymbol{f}}^*\right)$ and $\widehat{\boldsymbol{g}}\left(\widehat{\boldsymbol{x}}|\boldsymbol{\Theta}_{\boldsymbol{g}}^*\right)$. These functions are optimal estimated functions related to $\boldsymbol{f}(.)$ and $\boldsymbol{g}(.)$ realized by the optimal parameter vectors $\boldsymbol{\Theta}_{\boldsymbol{f}}^*$ and $\boldsymbol{\Theta}_{\boldsymbol{g}}^*$ such that:

$$\begin{aligned} \Theta_f^* &:= \underset{\Theta_f \in \mathbb{R}^{\prod_{i=1}^{n} p_i}}{\operatorname{argmin}} \left\{ \sup_{x \in \Omega} \left| \hat{f}\left(\hat{x}|\Theta_f^*\right) - f(x) \right| \right\} \\ \Theta_g^* &:= \underset{\Theta_g \in \mathbb{R}^{\prod_{i=1}^{n} q_i}}{\operatorname{argmin}} \left\{ \sup_{x \in \Omega} \left| \hat{g}\left(\hat{x}|\Theta_g^*\right) - g(x) \right| \right\} \end{aligned} \tag{30}$$

where the vector of parameters $\boldsymbol{\Theta}_{\boldsymbol{f}}$ and $\boldsymbol{\Theta}_{\boldsymbol{g}}$ are comprised of T2FNN parameters μ, σ_1, σ_2, w_v^i and w_s^i as defined in Section 3. Using Taylor's linearization, the difference between T2FNN estimated and optimal estimated functions related to $\boldsymbol{f}(.)$ and $\boldsymbol{g}(.)$ can be expressed as:

$$\widehat{\boldsymbol{f}}^*\left(\boldsymbol{x}|\boldsymbol{\Theta}_{\boldsymbol{f}}^*\right) - \widehat{\boldsymbol{f}}\left(\boldsymbol{x}|\boldsymbol{\Theta}_{\boldsymbol{f}}\right) = \left(\boldsymbol{\Theta}_{\boldsymbol{f}}^* - \boldsymbol{\Theta}_{\boldsymbol{f}}\right)^{\boldsymbol{T}} \left[\frac{\partial \widehat{\boldsymbol{f}}\left(\boldsymbol{x}|\boldsymbol{\Theta}_{\boldsymbol{f}}\right)}{\partial \boldsymbol{\Theta}_{\boldsymbol{f}}}\right] + h.o.t\left(\left|\boldsymbol{\Theta}_{\boldsymbol{f}}^* - \boldsymbol{\Theta}_{\boldsymbol{f}}\right|^2\right)$$

$$\widehat{\boldsymbol{g}}^{*}\left(\boldsymbol{x}|\boldsymbol{\Theta}_{\boldsymbol{g}}^{*}\right)-\widehat{\boldsymbol{g}}\left(\boldsymbol{x}|\boldsymbol{\Theta}_{\boldsymbol{g}}\right)=\left(\boldsymbol{\Theta}_{\boldsymbol{g}}^{*}-\boldsymbol{\Theta}_{\boldsymbol{g}}\right)^{T}\left[\frac{\partial\widehat{\boldsymbol{g}}\left(\boldsymbol{x}|\boldsymbol{\Theta}_{\boldsymbol{g}}\right)}{\partial\boldsymbol{\Theta}_{\boldsymbol{g}}}\right]+h.o.t\left(\left|\boldsymbol{\Theta}_{\boldsymbol{g}}^{*}-\boldsymbol{\Theta}_{\boldsymbol{g}}\right|^{2}\right) \tag{31}$$

where $h.o.t\left(\left|\boldsymbol{\Theta}_{\boldsymbol{f}}^{*}-\boldsymbol{\Theta}_{\boldsymbol{f}}\right|^{2}\right)$ and $h.o.t\left(\left|\boldsymbol{\Theta}_{\boldsymbol{g}}^{*}-\boldsymbol{\Theta}_{\boldsymbol{g}}\right|^{2}\right)$ represent higher order terms for each of the functions, respectively. Furthermore, the functions $\boldsymbol{f}(.)$ and $\boldsymbol{g}(.)$, being estimated by the T2FNN system, can be defined in terms of $\boldsymbol{\theta}_{\boldsymbol{f}}^{T}\boldsymbol{\xi}_{\boldsymbol{f}}(\boldsymbol{x})$ and $\boldsymbol{\theta}_{\boldsymbol{g}}^{T}\boldsymbol{\xi}_{\boldsymbol{g}}(\boldsymbol{x})$ with errors $\boldsymbol{\varepsilon}_{\boldsymbol{f}}(\boldsymbol{x})$ and $\boldsymbol{\varepsilon}_{\boldsymbol{g}}(\boldsymbol{x})$, respectively:

$$\begin{aligned}\widehat{\boldsymbol{f}}\left(\boldsymbol{x}|\boldsymbol{\Theta}_{\boldsymbol{f}}\right)&=\boldsymbol{\Theta}_{\boldsymbol{f}}^{T}\boldsymbol{\xi}_{\boldsymbol{f}}(\boldsymbol{x})+\boldsymbol{\varepsilon}_{\boldsymbol{f}}(\boldsymbol{x})\\ \widehat{\boldsymbol{g}}\left(\boldsymbol{x}|\boldsymbol{\Theta}_{\boldsymbol{g}}\right)&=\boldsymbol{\Theta}_{\boldsymbol{g}}^{T}\boldsymbol{\xi}_{\boldsymbol{g}}(\boldsymbol{x})+\boldsymbol{\varepsilon}_{\boldsymbol{g}}(\boldsymbol{x})\end{aligned} \tag{32}$$

where

$$\begin{aligned}\boldsymbol{\xi}_{\boldsymbol{f}}&=\frac{\partial\widehat{\boldsymbol{f}}\left(\boldsymbol{x}|\boldsymbol{\Theta}_{\boldsymbol{f}}\right)}{\partial\boldsymbol{\Theta}_{\boldsymbol{f}}}\\ \boldsymbol{\xi}_{\boldsymbol{g}}&=\frac{\partial\widehat{\boldsymbol{g}}\left(\boldsymbol{x}|\boldsymbol{\Theta}_{\boldsymbol{g}}\right)}{\partial\boldsymbol{\Theta}_{\boldsymbol{g}}}\end{aligned} \tag{33}$$

where $\boldsymbol{\Theta}_{\boldsymbol{f}}=\left[\Theta_{f1},\Theta_{f2},\cdots,\Theta_{fn}\right]$ and $\boldsymbol{\Theta}_{\boldsymbol{g}}=\left[\Theta_{g1},\Theta_{g2},\cdots,\Theta_{gn}\right]$ are the vectors of the tuning parameters and $\boldsymbol{\xi}_{\boldsymbol{f}}(\boldsymbol{x})=\left[\xi_{f1}(\boldsymbol{x}),\xi_{f2}(\boldsymbol{x}),\cdots,\xi_{fn}(\boldsymbol{x})\right]$ and $\boldsymbol{\xi}_{\boldsymbol{g}}(\boldsymbol{x})=\left[\xi_{g1}(\boldsymbol{x}),\xi_{g2}(\boldsymbol{x}),\cdots,\xi_{gn}(\boldsymbol{x})\right]$ are the T2FNN variable vectors.

The difference between the optimal function and T2FNN estimated function can be expressed as follows.

$$\begin{cases}\widehat{\boldsymbol{f}}^{*}\left(\boldsymbol{x}|\boldsymbol{\Theta}_{\boldsymbol{f}}^{*}\right)-\widehat{\boldsymbol{f}}\left(\boldsymbol{x}|\boldsymbol{\Theta}_{\boldsymbol{f}}\right)=\left(\boldsymbol{\Theta}_{\boldsymbol{f}}^{*}-\boldsymbol{\Theta}_{\boldsymbol{f}}\right)^{T}\boldsymbol{\xi}_{\boldsymbol{f}}+\boldsymbol{\varepsilon}_{\boldsymbol{f}}(\boldsymbol{x})=\widetilde{\boldsymbol{W}}\boldsymbol{\xi}_{\boldsymbol{f}}+\boldsymbol{\varepsilon}_{\boldsymbol{f}}(\boldsymbol{x})\\ \widehat{\boldsymbol{g}}^{*}\left(\boldsymbol{x}|\boldsymbol{\Theta}_{\boldsymbol{g}}^{*}\right)-\widehat{\boldsymbol{g}}\left(\boldsymbol{x}|\boldsymbol{\Theta}_{\boldsymbol{g}}\right)=\left(\boldsymbol{\Theta}_{\boldsymbol{g}}^{*}-\boldsymbol{\Theta}_{\boldsymbol{g}}\right)^{T}\boldsymbol{\xi}_{\boldsymbol{g}}+\boldsymbol{\varepsilon}_{\boldsymbol{g}}(\boldsymbol{x})=\widetilde{\boldsymbol{V}}\boldsymbol{\xi}_{\boldsymbol{g}}+\boldsymbol{\varepsilon}_{\boldsymbol{g}}(\boldsymbol{x})\end{cases} \tag{34}$$

From (21), it was concluded that the control law can both reach global asymptotic stability or a non-convergent stability with a steady-state tracking error since $\lim_{t\to\infty}\dot{\varepsilon}_{F}=0$. Therefore, a hierarchical switched controller is designed based on an exponential-like-sliding-mode T2FNN system.

Theorem 1. *The system presented in (12), is asymptotically stable by adaptation laws and control input chosen as follows:*

$$\begin{aligned}&\dot{\boldsymbol{\Theta}}_{\boldsymbol{f}}=-\gamma_{W}s_{2}\boldsymbol{\xi}_{\boldsymbol{f}}\left(\boldsymbol{x}|\boldsymbol{\Theta}_{\boldsymbol{f}}\right)\\ &\dot{\boldsymbol{\Theta}}_{\boldsymbol{g}}=-\gamma_{V}s_{3}\boldsymbol{\xi}_{\boldsymbol{g}}\left(\boldsymbol{x}|\boldsymbol{\Theta}_{\boldsymbol{g}}\right)\\ &\dot{\boldsymbol{\Theta}}_{\boldsymbol{D}}=-\gamma_{D}\xi_{5}\|\ \varepsilon_{F}\ \|_{\infty}\|\ \overline{\boldsymbol{D}}\ \|sign\left(\widetilde{\boldsymbol{D}}^{\boldsymbol{T}}\right)\\ &\delta_{f}=[h_{1}+h_{2}]h_{3}^{-1}-\lambda\dot{\varepsilon}_{F}-\xi_{1}\|\ \varepsilon_{F}\ \|_{\infty}e^{-\xi_{2}|s_{1}|}sign(s_{1})-\frac{\xi_{3}\|\varepsilon_{F}\|_{\infty}s_{1}}{\xi_{4}e^{-\xi_{1}|s_{1}|}}\end{aligned} \tag{35}$$

where γ_{W}, γ_{V}, and γ_{D} are the adaptation rates, ξ_{5} is a positive constant, s_{2} and s_{3} are multiple sliding surfaces and $\overline{\boldsymbol{D}}$ denotes the upper bound of the unknown but bounded disturbances.

Proof. Let us also denote the difference between optimal and estimated functions of T2FNN based on $\widetilde{\boldsymbol{D}}=\boldsymbol{D}-\hat{\boldsymbol{D}}(\boldsymbol{\Theta}_{\boldsymbol{D}})$, where $\boldsymbol{D}$ is the external disturbance, $\widehat{\boldsymbol{D}}(\boldsymbol{\Theta}_{\boldsymbol{D}})$ is the estimated disturbance as a function of the adaptive parameter $\boldsymbol{\Theta}_{\boldsymbol{D}}$. Also, consider multiple sliding surfaces:

$$\begin{aligned}s_{1}&=\dot{\varepsilon}_{F}+\lambda\varepsilon_{F}\\ s_{2}&=\int_{0}^{t}\widetilde{\boldsymbol{W}}^{\boldsymbol{T}}\ \boldsymbol{\xi}_{\boldsymbol{f}}(\boldsymbol{x})+\boldsymbol{\varepsilon}_{\boldsymbol{f}}(\boldsymbol{x})d\tau\\ s_{3}&=\int_{0}^{t}\widetilde{\boldsymbol{V}}^{\boldsymbol{T}}\ \boldsymbol{\xi}_{\boldsymbol{g}}(\boldsymbol{x})+\boldsymbol{\varepsilon}_{\boldsymbol{g}}(\boldsymbol{x})d\tau\end{aligned} \tag{36}$$

where λ is a positive constant. The conventional reaching law for the sliding surface, $\dot{s}_{1}=-\xi_{1}sign(s_{1})-\xi_{2}s_{1}$ with $\xi_{1}$and ξ_{2} being positive constants, degrades the system stability and introduces an inherent chattering of the controller input. Additionally, there is a buffeting switch zone close to the origin [40], an updated globally asymptotic reaching law is thus employed here such that:

$$\dot{s}_{1}=-\xi_{1}\|\ \varepsilon_{F}\ \|_{\infty}e^{-\xi_{2}|s_{1}|}sign(s_{1})-\frac{\xi_{3}\|\ \varepsilon_{F}\ \|_{\infty}s_{1}}{\xi_{4}e^{-\xi_{1}|s_{1}|}} \tag{37}$$

where ξ_1, ξ_2, ξ_3 and ξ_4 are arbitrary positive constants and $\| \varepsilon_F \|_\infty$ is the infinity norm of the system where $\lim_{t\to\infty} \| \varepsilon_F \|_\infty = 0$. Consider a Lyapunov candidate function such as:

$$V_4(t) = \frac{1}{2}s_1^2 + \frac{1}{2}s_2^2 + \frac{1}{2}s_3^2 + \frac{1}{2\gamma_W}\tilde{\boldsymbol{W}}\,\tilde{\boldsymbol{W}}^{\boldsymbol{T}} + \frac{1}{2\gamma_V}\tilde{\boldsymbol{V}}\,\tilde{\boldsymbol{V}}^{\boldsymbol{T}} + \frac{1}{2\gamma_D}\tilde{\boldsymbol{D}}\,\tilde{\boldsymbol{D}}^{\boldsymbol{T}} \tag{38}$$

By taking the time derivative of $V_4(t)$:

$$\begin{aligned}\dot{V}_4(t) &= s_1\dot{s}_1 + s_2\dot{s}_2 + s_3\dot{s}_3 - \frac{1}{\gamma_W}\dot{\tilde{\boldsymbol{W}}}\tilde{\boldsymbol{W}}^{\boldsymbol{T}} - \frac{1}{\gamma_V}\dot{\tilde{\boldsymbol{V}}}\tilde{\boldsymbol{V}}^{\boldsymbol{T}} - \frac{1}{\gamma_D}\dot{\tilde{\boldsymbol{D}}}\tilde{\boldsymbol{D}}^{\boldsymbol{T}} \\ &= -\xi_1\| \varepsilon_F \|_\infty e^{-\xi_2|s_1|}|s_1| - s_1^2\frac{\xi_3\| \varepsilon_F \|_\infty}{\xi_4 e^{-\xi_1|s_1|}} + \left(\tilde{\boldsymbol{W}}^{\boldsymbol{T}}\boldsymbol{\xi_f}(\boldsymbol{x}) + \boldsymbol{\varepsilon_f}(\boldsymbol{x})\right)s_2 + \left(\tilde{\boldsymbol{V}}^{\boldsymbol{T}}\boldsymbol{\xi_g}(\boldsymbol{x}) + \boldsymbol{\varepsilon_g}(\boldsymbol{x})\right)s_3 - \frac{1}{\gamma_W}\dot{\tilde{\boldsymbol{W}}}\tilde{\boldsymbol{W}}^{\boldsymbol{T}} \\ &\quad - \frac{1}{\gamma_V}\dot{\tilde{\boldsymbol{V}}}\tilde{\boldsymbol{V}}^{\boldsymbol{T}}\end{aligned} \tag{39}$$

Considering that the function approximation errors $\boldsymbol{\varepsilon_f}(\boldsymbol{x})$ and $\boldsymbol{\varepsilon_f}(\boldsymbol{x})$ are small bounded magnitudes, it can be shown that $\| \boldsymbol{\varepsilon_f}(\boldsymbol{x})s_2 + \boldsymbol{\varepsilon_g}(\boldsymbol{x})s_3 \| \ll \eta$ where η is the appropriate and strictly positive gain factor. By adding a positive term $\eta \le \xi_5\| \varepsilon_F \|_\infty \| \tilde{\boldsymbol{D}}^{\boldsymbol{T}}\overline{\boldsymbol{D}} \|$, (39) can be rewritten as:

$$\begin{aligned}\dot{V}_4(t) \le &-\xi_1\| \varepsilon_F \|_\infty e^{-\xi_2|s_1|}|s_1| - s_1^2\frac{\xi_3\| \varepsilon_F \|_\infty}{\xi_4 e^{-\xi_1|s_1|}} + \left(\tilde{\boldsymbol{W}}^{\boldsymbol{T}}\boldsymbol{\xi_f}(\boldsymbol{x})\right)s_2 + \left(\tilde{\boldsymbol{V}}^{\boldsymbol{T}}\boldsymbol{\xi_g}(\boldsymbol{x})\right)s_3 - \eta - \frac{1}{\gamma_W}\dot{\tilde{\boldsymbol{W}}}\tilde{\boldsymbol{W}}^{\boldsymbol{T}} - \frac{1}{\gamma_V}\dot{\tilde{\boldsymbol{V}}}\tilde{\boldsymbol{V}}^{\boldsymbol{T}} - \frac{1}{\gamma_D}\dot{\tilde{\boldsymbol{D}}}\tilde{\boldsymbol{D}}^{\boldsymbol{T}} \\ &+ \xi_5\| \varepsilon_F \|_\infty\tilde{\boldsymbol{D}}^{\boldsymbol{T}} \| \overline{\boldsymbol{D}} \| sign\left(\tilde{\boldsymbol{D}}^{\boldsymbol{T}}\right)\end{aligned} \tag{40}$$

Equation (40) can be rewritten according to the time derivative of the vectors of the training parameters T2FNN system $\boldsymbol{\Theta_f}$, $\boldsymbol{\Theta_g}$ and $\boldsymbol{\Theta_D}$ related to the functions of $\boldsymbol{f}(.)$, $\boldsymbol{g}(.)$ and disturbance $\boldsymbol{D}$ such that:

$$\begin{aligned}\dot{V}_4(t) \le &-\xi_1\| \varepsilon_F \|_\infty e^{-\xi_2|s_1|}|s_1| - s_1^2\frac{\xi_3\| \varepsilon_F \|_\infty}{\xi_4 e^{-\xi_1|s_1|}} + \left(\tilde{\boldsymbol{W}}^{\boldsymbol{T}}\boldsymbol{\xi_f}(\boldsymbol{x})\right)s_2 + \left(\tilde{\boldsymbol{V}}^{\boldsymbol{T}}\boldsymbol{\xi_g}(\boldsymbol{x})\right)s_3 - \eta - \frac{1}{\gamma_W}\dot{\boldsymbol{\Theta}}_{\boldsymbol{f}}\tilde{\boldsymbol{W}}^{\boldsymbol{T}} - \frac{1}{\gamma_V}\dot{\boldsymbol{\Theta}}_{\boldsymbol{g}}\tilde{\boldsymbol{V}}^{\boldsymbol{T}} \\ &- \frac{1}{\gamma_D}\dot{\boldsymbol{\Theta}}_{\boldsymbol{D}}\tilde{\boldsymbol{D}}^{\boldsymbol{T}} + \xi_5\| \varepsilon_F \|_\infty\tilde{\boldsymbol{D}}^{\boldsymbol{T}} \| \overline{\boldsymbol{D}} \| sign\left(\tilde{\boldsymbol{D}}^{\boldsymbol{T}}\right)\end{aligned} \tag{41}$$

By considering the adaptation laws according to (35), (41) is reduced to:

$$\dot{V}_4(t) \le -\xi_1\| \varepsilon_F \|_\infty e^{-\xi_2|s_1|}|s_1| - s_1^2\frac{\xi_3\| \varepsilon_F \|_\infty}{\xi_4 e^{-\xi_1|s_1|}} - \eta \le 0 \tag{42}$$

In which case, the closed-loop system is globally asymptotically stable and the convergence of the tracking error ε_F to zero in finite time is ensured in a robust manner. This completes the proof. ■

5. Simulation results

The effectiveness of the proposed adaptive robust control method is evaluated considering simulation scenarios involving two different maneuvers: a double lane change (DLC) and an S-curve (Fig. 3). The simulation scheme involving CarSim and MATLAB/Simulink co-simulations is also shown in Fig. 3. The simulation parameters are summarized in Table 1. The simulations are performed considering the road adhesion coefficient $\mu_t = 0.5$ and different constant forward velocities (v_x = 10, 20 and 30 m/s). The robustness of the proposed controller is also examined considering parametric uncertainties related to the tire cornering stiffness, road-tire adhesion coefficient and inertial parameters. These are represented by ±10% perturbation about the respective nominal values, using a 2 Hz sinusoidal function together with a raised-cosine pulse at t = 2 s to account for the effect of sudden external disturbances. The purpose of the proposed controller is to achieve asymptotic convergence of the vehicle path-tracking error comprising an adaptive look-ahead term toward zero, while preserving the stability of the closed-loop system. The RMS and maximum ε_F together with the heading error ($\Delta\varphi$) are taken as the performance metrics for evaluating the proposed controller. In order to compare the effectiveness of the proposed controller, a type-1 fuzzy neural network (T1FNN) controller is also formulated and results are compared with those obtained with the proposed controller to further examine the relative effectiveness of the proposed method. The simulation results are further compared with those of a linear quadratic regulator (LQT) and an active disturbance rejection control (ADRC) method, reported in [41]. The look-ahead time can be defined based on a variable speed look-ahead distance model [42]:

$$\Xi = \frac{4v_x m l_1}{\widehat{C}_R(l_1 + l_2)} - \frac{l_2}{v_x} \tag{43}$$

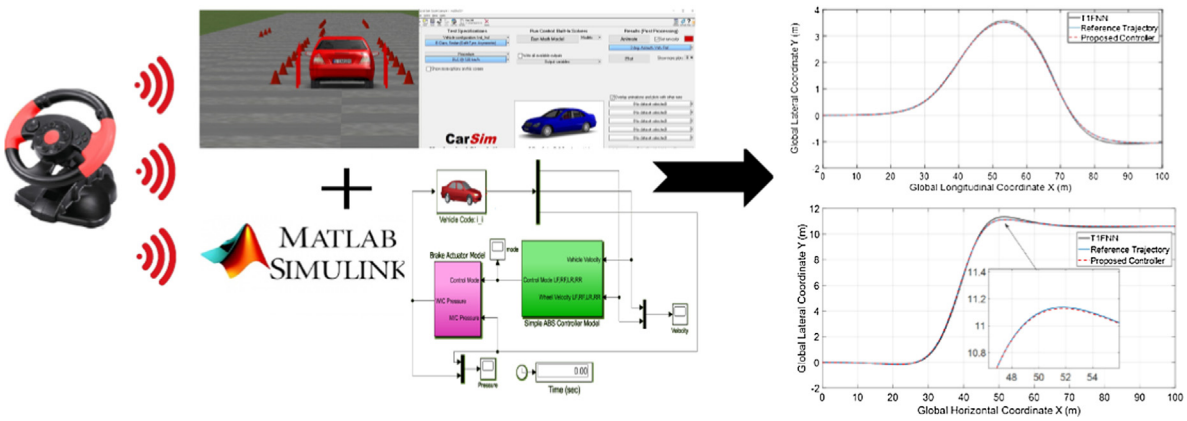

Fig. 3. CarSim-Matlab co-simulation platform for autonomous path-tracking control.

Table 1
Simulation parameters [41].

Parameter (Unit)	Value
m, kg	1480
I_z, kgm^2	2350
l_1, m	1.05
l_2, m	1.63
$\widehat{C}_F$, N/rad	67,500
$\widehat{C}_R$, N/rad	74,500

In which case, the look-ahead time for the vehicle at the nominal operating speed, v_x = 10, is about 0.2 s. A safety factor of 2 is used in order to regulate further distant look-ahead error.

A. DLC simulation

The autonomous vehicle and controller responses to the DLC maneuver are evaluated under nominal forward speed ($v_x = 10$ m/s) on a road with relatively lower adhesion coefficient ($\mu_t = 0.5$). The lateral offset for the proposed controller is compared with that obtained using the T1FNN controller (Fig. 4). The results show that the T1FNN controller yields lateral offset magnitude within the range, $|\varepsilon_F| < 0.25$ m, which is considerably larger than that obtained by the proposed controller ($|\varepsilon_F| < 0.05$ m). The proposed controller holds the capacity to stabilize the path following error swiftly without any steady-state error, which is primarily due to exponential-like sliding surface level of the hierarchical controller. A similar trend is also observed in the heading error response of autonomous vehicle with the proposed and T1FNN controllers, as seen in Fig. 4(b). It is evident that the T1FNN controller yields substantial errors during each path-change of the DLC maneuver, while the variations the heading angle responses of both the controllers are consistent with the path curvature. The superior performance benefit of the proposed method is especially notable in the transient lateral-offset response, which is of greater significance during critical maneuvers such as lane changing or collision avoidance. The path-tracking performance of the autonomous vehicle in the global coordinate system is also illustrated in Fig. 4(c). The proposed controller tracks the desired trajectory during the entire simulation period with the absence of overshoot and steady-state error. However, the T1FNN controller returns to the desired trajectory after the two overshoots between 55–65 m and 75–95 m of the longitudinal travel, which may be indicative of lower damping characteristics of the trained T1FNN system.

Fig. 5 illustrates the control effort and the vehicle yaw-rate together with the lateral acceleration responses of the vehicle with the T1FNN and the proposed controllers. The control demand, presented in terms of steer angle, is considerably smaller for proposed controller compared to the T1FNN method, especially in the peak demand regions. This can be attributed to the switched hierarchical control strategy which contributes to a decrease in control effort according to the dynamics of tracking error. A similar trend is observed for the vehicle yaw-rate variations obtained from the two control strategies. The proposed method also maintains vehicle yaw-rate within a relatively smaller bound, which contributes to lower tire side-slip and thereby lower lateral force demand in undertaking the desired maneuver. The smooth variations in lateral acceleration response in the transient mode and during the entire simulation range is the result of a smooth asymptotically convergent steering input of the exponential-like-sliding-mode T2FNN controller when compared to the T1FNN controller (Fig. 5(c)).

The results obtained from the proposed controller are also compared with those obtained from the ADRC and LQT algorithms [41] in Table 2 for the DLC maneuver in terms of rms and maximum values of path-tracking performance. It is evident

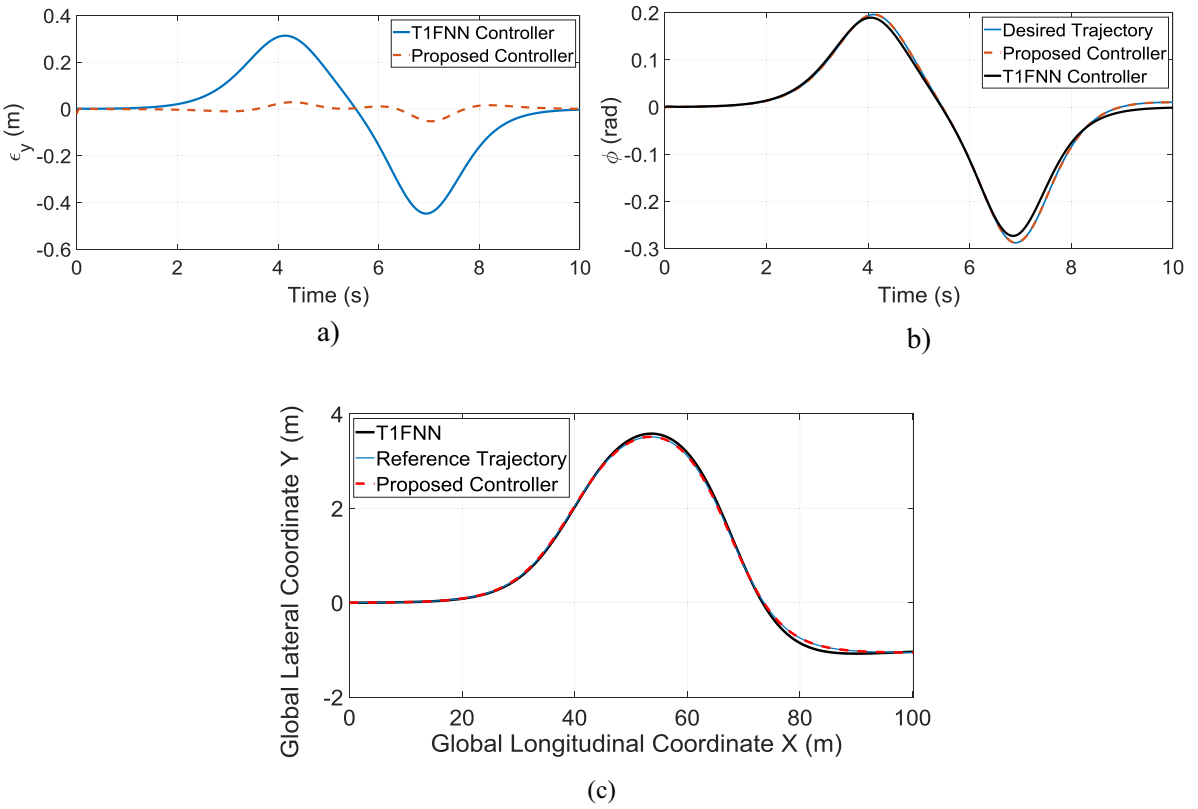

Fig. 4. Comparisons of a) lateral offset; b) heading angle trajectory-tracking; and c) global lateral position tracking performance of the proposed controller and T1FNN approach without a disturbance.

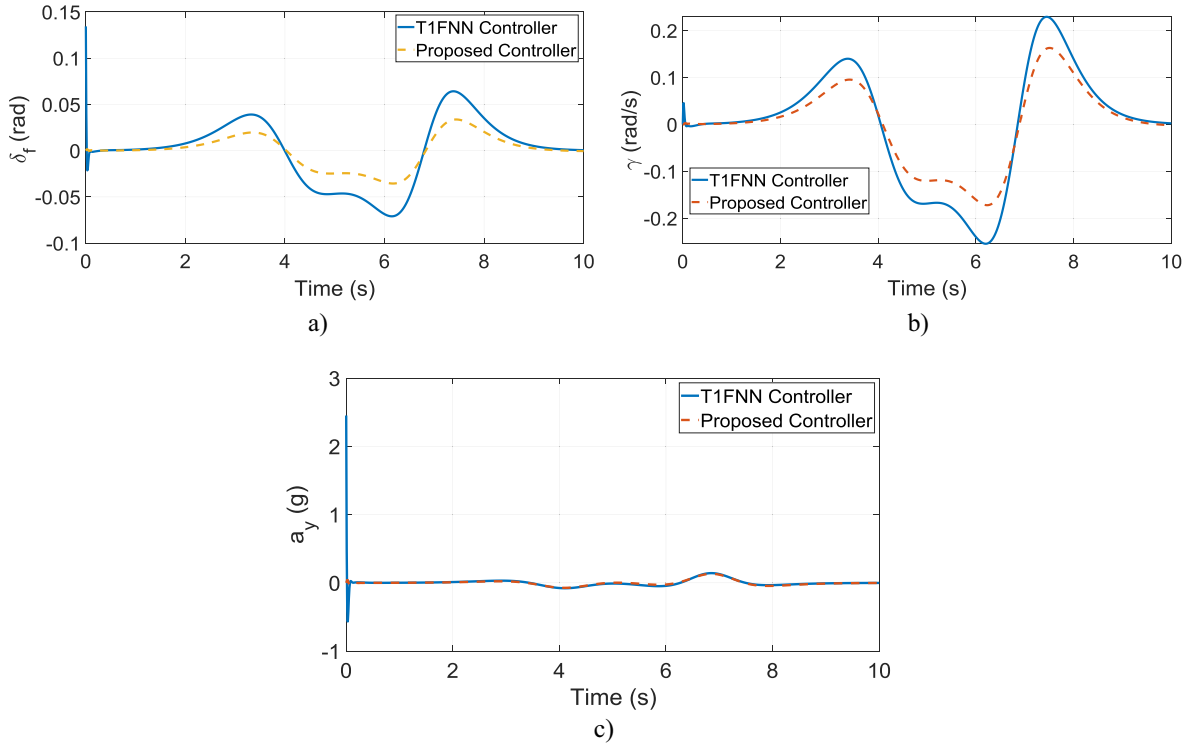

Fig. 5. Comparisons of: a) control effort; b) yaw-rate; and c) lateral acceleration responses of the proposed controller and T1FNN approach without a disturbance.

Table 2
Comparisons of rms and maximum values of tracking errors obtained from the proposed controller and the ADRC and LQT [41] methods.

Performance Metric	ADRC	LQT	Proposed method
rms ε_F (m)	0.2207	1.1049	0.0188
maximum ε_F (m)	0.5592	1.7757	0.0292
rms $\Delta\varphi$ (rad)	0.0178	0.0592	0.0016
maximum $\Delta\varphi$ (rad)	0.0363	0.1456	0.0019

that the proposed controller yields substantially lower lateral offset and the heading angle errors compared to the ADRC and LQT (Linear Quadratic Tracking) methods. The LQT method reported in [41] yields the highest tracking errors compared to the other methods considered. Moreover, the LQT method is known to exhibit certain limitations for typical disturbed linear systems and external disturbances.

The lateral stability of the vehicle is strongly affected by the forward speed, which imposes considerable variations in the lateral force and centrifugal acceleration in addition to the look-ahead time as it is evident from (43). The tracking performance of the autonomous vehicle is thus further evaluated considering the DLC maneuver at relatively higher speeds of 20 m/s and 30 m/s, and the influences on the performance metrics of the vehicle with the proposed controller are summarized in Table 3. The DLC maneuver at a higher speed requires its completion within a shorter time span, and thereby more abrupt path changes. Such maneuvers impose more complex path tracking performance demand for the controller achieve low as well as high damping ratios for tracking the trajectory swiftly, and for minimizing the overshoot and steady-state error, respectively. The rms and peak tracking errors observed for different forward speeds, considered as the performance metrics, are summarized in Table 3. The results suggest only slightly higher tracking errors with increasing speed, although more abrupt path changes are performed at higher speeds. Despite the slight increase in the tracking error, the proposed controller revealed superior path tracking during the entire simulation span in a robust manner.

The robustness of the proposed controller is also investigated considering parametric uncertainties related to the tire cornering stiffness, road-tire adhesion coefficient and inertial parameters. These parameters are perturbed ±10% about the respective nominal values using a 2 Hz sinusoidal function. Furthermore, a raised-cosine pulse signal starting at $t = 2$ s is introduced to examine robustness against sudden variations in the external disturbance applied to the system. The performance of the proposed and T1FNN controllers are compared to evaluate the relative effects of integrated uncertainty and external disturbance. Fig. 6 illustrates the controllers' responses in terms of control input, lateral acceleration and lateral offset error. It can be seen that the perturbed parameters significantly affect the transient performance of the T1FNN in terms of the controller demand. The lateral acceleration of the vehicle in the transient state is thus considerably higher. While the control effort for the proposed controller exhibits smooth variations in the transient state at the onset of the motion, it is slightly higher in the vicinity of the steering reversals when compared to that of the T1FNN control. Moreover, the proposed controller yields only slightly higher lateral path-tracking error in the presence of the uncertainties and external disturbance, while the T1FNN approach exhibits substantially higher path error, as evident in Fig. 6(c). This is partly due to the switched hierarchical control strategy and the smooth global asymptotic stability of the proposed adaptive control law together with the robustness of the fuzzy type-2 sets.

B. S-curve simulation

The performance of the proposed controller is further evaluated under an S-Curve maneuver at the nominal forward speed ($v_x = 10$ m/s) on a relatively low adhesion road surface ($\mu_t = 0.5$). The control demand and vehicle yaw-rate responses obtained for the two control strategies are compared in Fig. 7. The results further confirm smooth variations in the control signal of the proposed controller at the onset of the lateral motion of the vehicle. Substantially higher control effort, however, is evident for the T1FNN controller in the transient state, as seen in Fig. 7(a). The exponential-like-sliding-mode T2FNN controller resulted in rapid path following response with lower overshoots and steady-state errors when compared to the T1FNN counterpart. This is also evident from substantially higher peak yaw-rate response of the vehi-

Table 3
Comparison of RMS and maximum values for tracking errors at different longitudinal speeds.

Performance Metric	10 m/s	20 m/s	30 m/s
rms ε_F (m)	0.0188	0.0852	0.1012
maximum ε_F (m)	0.0292	0.1196	0.1385
rms $\Delta\varphi$ (rad)	0.0016	0.0021	0.0026
maximum $\Delta\varphi$ (rad)	0.0019	0.0029	0.0033

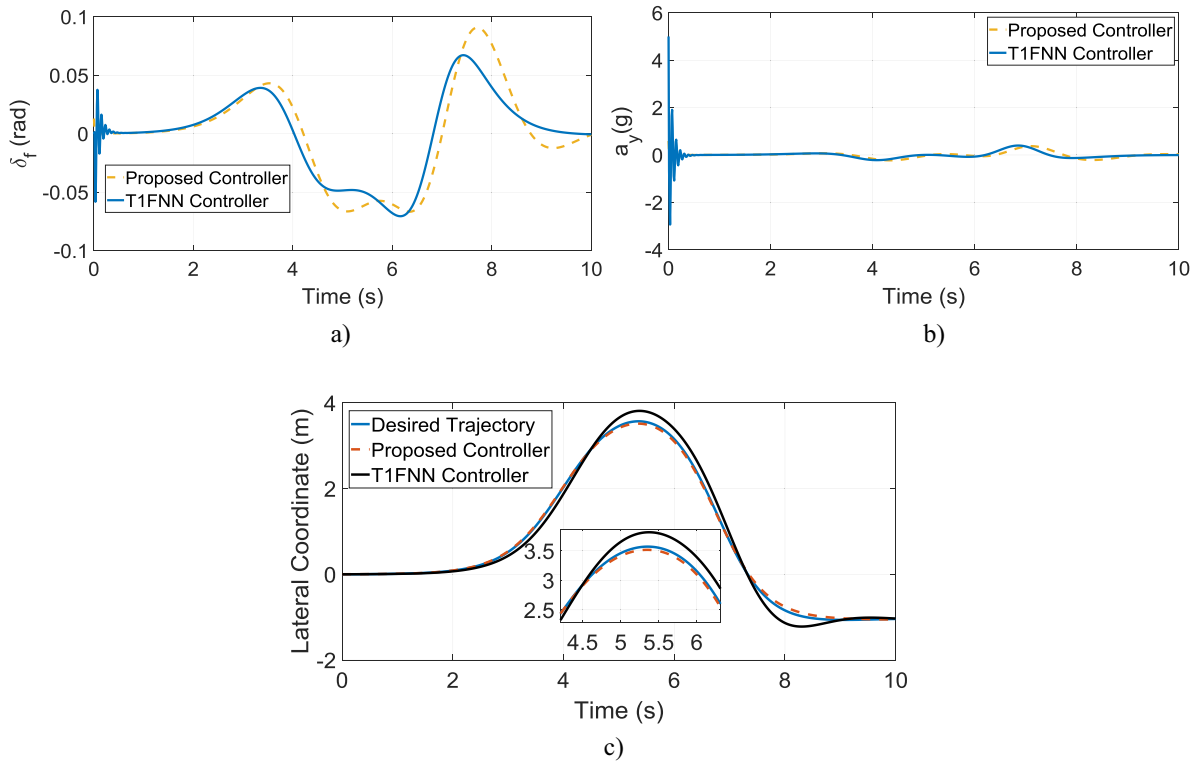

Fig. 6. Comparisons of: a) control effort; b) lateral acceleration; and c) global lateral position responses of the vehicle with the proposed controller and the T1FNN approach in the presence of a disturbance.

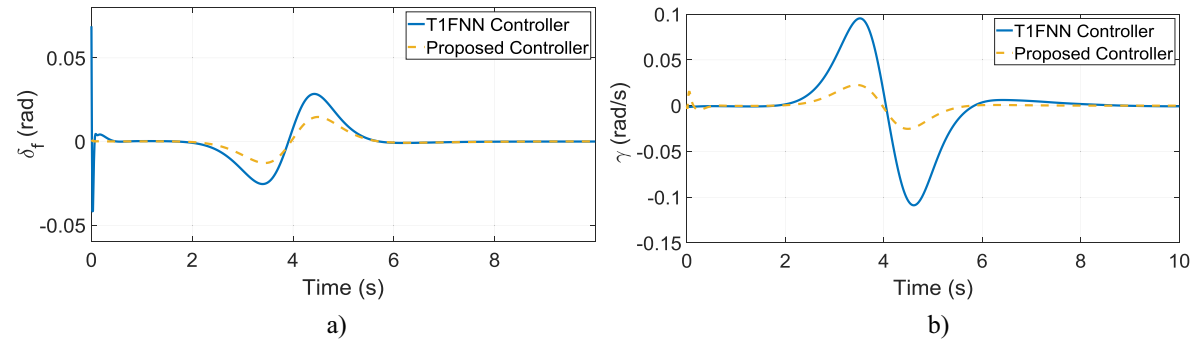

Fig. 7. Comparisons of: a) control demand; and b) vehicle yaw-rate response obtained with the proposed and T1FNN control strategies during an S-curve maneuver.

cle employing the T1FNN controller, which is nearly 5 times greater than that obtained with the proposed controller. This contributes to considerably higher heading angle error of the T1FNN control method when compared to the proposed control, as seen in Fig. 8(a). It should be noted that the heading error does not converge to zero for both the control frameworks, which is attributed to the requirement of a nonzero side-slip angle for smooth tracking of the curved path. Large heading angle error also contributes to a substantially higher lateral offset of the T1FNN controller, as seen in Fig. 8(b). The peak lateral offset approaches as high as 0.21 m, which is significantly higher than 0.02 m obtained for the proposed controller. The path-following performance of the two control methods in the global coordinates is also compared in Fig. 8(c). The results suggest only marginal tracking error of the proposed method with negligible overshoot and steady-state error.

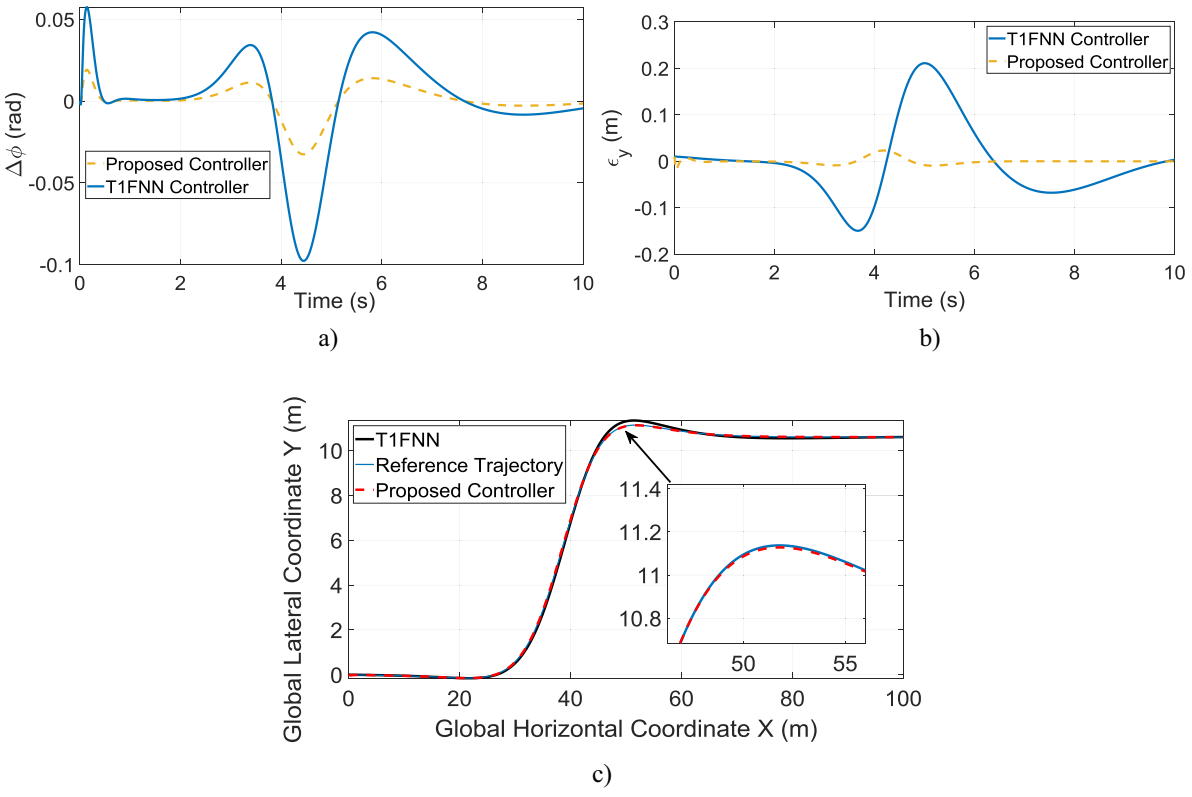

Fig. 8. Comparisons of: a) vehicle heading angle error; b) lateral offset; and c) global lateral position of the autonomous vehicle employing the proposed and T1FNN controllers (S-curve maneuver).

6. Conclusion

The path-following of autonomous vehicles continues of considerable interest due to hard system nonlinearities, disturbances, modeled and unstructured uncertainties, and input saturation, which directly affect the tracking error and stability of the vehicle. This study proposed two approaches to address path-following via kinematic model adjustments, and via a control algorithm development. Firstly, a quadratic error term based on the heading angle error is introduced for predicting future lateral offset errors using the kinematics response of the model. This model correction is subsequently employed to enhance the path following process based on a look-ahead strategy, which can considerably decrease the overall steady-state errors related to the vehicle lateral offset. Secondly, a hierarchical control scheme is proposed for the robust disturbance rejection performance of the vehicle arising from the environment and the uncertainties related to the parameter perturbations. The reaching law related to the sliding mode degrades the system stability and introduces an inherent chattering of the controller input. Additionally, there is a buffeting switch zone close to the origin, and thereby the convergence law for the sliding surface is adjusted in this paper based on a variable exponential sliding law. Simulation results obtained under different directional maneuvers at different speeds demonstrated superior path-following performance of the proposed control method when compared to other reported methods.

References

[1] X. Hu, H. Wang, X. Tang, Cyber-physical control for energy-saving vehicle following with connectivity, IEEE Trans. Ind. Electron. 64 (11) (2017) 8578–8587.
[2] H. Guo, C. Shen, H. Zhang, H. Chen, R. Jia, Simultaneous trajectory planning and tracking using an MPC method for cyber-physical systems: a case study of obstacle avoidance for an intelligent vehicle, IEEE Trans. Ind. Inform. 14 (9) (Sept. 2018) 4273–4283.
[3] J. Guo, Y. Luo, K. Li, An adaptive hierarchical trajectory following control approach of autonomous four-wheel independent drive electric vehicles, IEEE Trans. Intell. Transp. Syst. 19 (8) (2018) 2482–2492.
[4] C. Hu, H. Jing, R. Wang, F. Yan, M. Chadli, Robust H∞ output-feedback control for path following of autonomous ground vehicles, Mech. Syst. Signal Process. 70 (2016) 414–427.
[5] H. Guo, L. Song, J. Liu, F.Y. Wang, D. Cao, H. Chen, P.C.K. Luk, Hazard-evaluation-oriented moving horizon parallel steering control for driver-automation collaboration during automated driving, IEEE/CAA J. Autom. Sin. 5 (6) (2018) 1062–1073.
[6] H. Guo, D. Cao, H. Chen, Z. Sun, Y. Hu, Model predictive path following control for autonomous cars considering a measurable disturbance: implementation, testing, and verification, Mech. Syst. Signal Process. 118 (2019) 41–60.

[7] M. Zhu, H. Chen, G. Xiong, A model predictive speed tracking control approach for autonomous ground vehicles, Mech. Syst. Signal Process. 87 (2017) 138–152.
[8] J.E. Naranjo, C. Gonzalez, R. Garcia, T. de Pedro, Lane-change fuzzy control in autonomous vehicles for the overtaking maneuver, IEEE Trans. Intell. Transp. Syst. 9 (3) (Sep. 2008) 438–450.
[9] J. Wang, J. Wang, R. Wang, C. Hu, A framework of vehicle trajectory replanning in lane exchanging with considerations of driver characteristics, IEEE Trans. Veh. Technol. 66 (5) (2017) 3583–3596.
[10] A.P. Aguiar, J.P. Hespanha, Trajectory-tracking and path-following of underactuated autonomous vehicles with parametric modeling uncertainty, IEEE Trans. Autom. Control 52 (8) (2007) 1362–1379.
[11] C. Hu, Y. Qin, H. Cao, X. Song, K. Jiang, J.J. Rath, C. Wei, Lane keeping of autonomous vehicles based on differential steering with adaptive multivariable super-twisting control, Mech. Syst. Signal Process. 125 (2019) 330–346.
[12] C. Hu, R. Wang, F. Yan, N. Chen, Should the desired heading in path following of autonomous vehicles be the tangent direction of the desired path?, IEEE Trans Intell. Transp. Syst. 16 (6) (2015) 3084–3094.
[13] C. Hu, R. Wang, F. Yan, N. Chen, Output constraint control on path following of four-wheel independently actuated autonomous ground vehicles, IEEE Trans. Veh. Technol. 65 (6) (2016) 4033–4043.
[14] X. Li, Z. Sun, D. Cao, D. Liu, H. He, Development of a new integrated local trajectory planning and tracking control framework for autonomous ground vehicles, Mech. Syst. Signal Process. 87 (part B) (2017) 118–137.
[15] R. Wang, C. Hu, F. Yan, M. Chadli, Composite nonlinear feedback control for path following of four-wheel independently actuated autonomous ground vehicles, IEEE Trans. Intell. Transp. Syst. 17 (7) (2016) 2063–2074.
[16] X. Ji, X. He, C. Lv, Y. Liu, J. Wu, Adaptive-neural-network-based robust lateral motion control for autonomous vehicle at driving limits, Control Eng. Pract. 76 (2018) 41–53.
[17] Rongrong Wang, Hui Jing, Hu. Chuan, Fengjun Yan, Nan Chen, Robust H∞ path following control for autonomous ground vehicles with delay and data dropout, IEEE Trans. Intell. Transp. Syst. 17 (7) (2016) 2042–2050.
[18] S.E. Li, K. Deng, K. Li, C. Ahn, Terminal sliding mode control of automated car-following system without reliance on longitudinal acceleration information, Mechatronics 30 (2015) 327–337.
[19] Q. Cui, R. Ding, B. Zhou, X. Wu, Path-tracking of an autonomous vehicle via model predictive control and nonlinear filtering, Proc. Inst. Mech. Eng., Part D: J. Automobile Eng. (2017), 0954407017728199.
[20] Hongyan Guo, Feng Liu, Xu. Fang, Hong Chen, Dongpu Cao, Yan Ji, Nonlinear model predictive lateral stability control of active chassis for intelligent vehicles and its FPGA implementation, IEEE Trans. Syst. Man Cybern.: Syst. 99 (2017) 1–12.
[21] H. Zhang, J. Wang, Active steering actuator fault detection for an automatically-steered electric ground vehicle, IEEE Trans. Veh. Technol. 66 (5) (2017) 3685–3702.
[22] Xiangyang Xu, Yinghua Liang, Mick Jordan, Peter Tenberge, Peng Dong, Optimized control of engine start assisted by the disconnect clutch in a P2 hybrid automatic transmission, Mech. Syst. Signal Process. 124 (2019) 313–329.
[23] X. Du, K.K. Tan, Autonomous reverse parking system based on robust path generation and improved sliding mode control, IEEE Trans. Intell. Transp. Syst. 16 (3) (2015) 1225–1237.
[24] D. Xu, Y. Shi, Z. Ji, Model-free adaptive discrete-time integral sliding-mode-constrained-control for autonomous 4WMV parking systems, IEEE Trans. Ind. Electron. 65 (1) (2018) 834–843.
[25] C. Hu, R. Wang, F. Yan, H.R. Karimi, Robust composite nonlinear feedback path-following control for independently actuated autonomous vehicles with differential steering, IEEE Trans. Transp. Electrif. 2 (3) (2016) 312–321.
[26] N.H. Amer, H. Zamzuri, K. Hudha, Z.A. Kadir, Modelling and control strategies in path tracking control for autonomous ground vehicles: a review of state of the art and challenges, J. Intell. Rob. Syst. 86 (2) (2017) 225–254.
[27] W. He, Y. Chen, Z. Yin, Adaptive neural network control of an uncertain robot with full-state constraints, IEEE Trans. Cybern. 46 (3) (2016) 620–629.
[28] S. Ghaffari, M.R. Homaeinezhad, Autonomous path following by fuzzy adaptive curvature-based point selection algorithm for four-wheel-steering car-like mobile robot, Proc. Inst. Mech. Eng., Part C: J. Mech. Eng. Sci. 232 (15) (2018) 2655–2665.
[29] S. Yang, Y. Cao, Z. Peng, G. Wen, K. Guo, Distributed formation control of nonholonomic autonomous vehicle via RBF neural network, Mech. Syst. Signal Process. 87 (2017) 81–95.
[30] X. Wang, M. Fu, H. Ma, Y. Yang, Lateral control of autonomous vehicles based on fuzzy logic, Control Eng. Pract. 34 (2015) 1–17.
[31] C. Zhang, J. Hu, J. Qiu, W. Yang, H. Sun, Q. Chen, A Novel fuzzy observer-based steering control approach for path tracking in autonomous vehicles, IEEE Trans. Fuzzy Syst. (2018).
[32] J.P. Rastelli, M.S. Peñas, Fuzzy logic steering control of autonomous vehicles inside roundabouts, Appl. Soft Comput. 35 (2015) 662–669.
[33] C.L. Hwang, C.C. Yang, J.Y. Hung, Path tracking of an autonomous ground vehicle with different payloads by hierarchical improved fuzzy dynamic sliding-mode control, IEEE Trans. Fuzzy Syst. 26 (2) (2018) 899–914.
[34] A. Mohammadzadeh, O. Kaynak, M. Teshnehlab, Two-mode indirect adaptive control approach for the synchronization of uncertain chaotic systems by the use of a hierarchical interval type-2 fuzzy neural network, IEEE Trans. Fuzzy Syst. 22 (5) (2014) 1301–1312.
[35] M.A. Khanesar, E. Kayacan, M. Teshnehlab, O. Kaynak, Analysis of the noise reduction property of type-2 fuzzy logic systems using a novel type-2 membership function, IEEE Trans. Syst. Man Cybern. Part B (Cybern.) 41 (5) (2011) 1395–1406.
[36] C. Ahn, H. Peng, H.E. Tseng, Robust estimation of road frictional coefficient, IEEE Trans. Control Syst. Technol. 21 (1) (2013) 1–13.
[37] M.M. Zirkohi, T.C. Lin, Interval type-2 fuzzy-neural network indirect adaptive sliding mode control for an active suspension system, Nonlinear Dyn. 79 (1) (2015) 513–526.
[38] A. Mohammadzadeh, S. Ghaemi, A modified sliding mode approach for synchronization of fractional-order chaotic/hyperchaotic systems by using new self-structuring hierarchical type-2 fuzzy neural network, Neurocomputing 191 (2016) 200–213.
[39] J.M. Mendel, Type-2 fuzzy logic systems, IEEE Trans. Fuzzy Syst. 7 (1999) 643–658.
[40] J.J.E. Slotine, W. Li, Applied Nonlinear Control (Vol. 199, No. 1), Prentice Hall, Englewood Cliffs, NJ, 1991.
[41] Y. Xia, F. Pu, S. Li, Y. Gao, Lateral path tracking control of autonomous land vehicle based on ADRC and differential flatness, IEEE Trans. Ind. Electron. 63 (5) (2016) 3091–3099.
[42] P. Hingwe, M. Tomizuka, A variable look-ahead controller for lateral guidance of four wheeled vehicles June, in: American Control Conference, 1998. Proceedings of the 1998, IEEE, 1998, pp. 31–35.